

# Budget-Aware Activity Detection with A Recurrent Policy Network

Behrooz Mahasseni<sup>1,2,\*</sup> Xiaodong Yang<sup>2</sup> Pavlo Molchanov<sup>2</sup> Jan Kautz<sup>2</sup>  
<sup>1</sup>Oregon State University <sup>2</sup>NVIDIA Research

## Abstract

*In this paper, we address the challenging problem of efficient temporal activity detection in untrimmed long videos. While most recent work has focused and advanced the detection accuracy, the inference time can take seconds to minutes in processing one video, which is computationally prohibitive for many applications with tight runtime constraints. This motivates our proposed budget-aware framework, which learns to perform activity detection by intelligently selecting a small subset of frames according to a specified time or computational budget. We formulate this problem as a Markov decision process, and adopt a recurrent network to model a policy for the frame selection. To train the network, we employ a recurrent policy gradient approach to approximate the gradient of the non-decomposable and non-differentiable objective defined in our problem. In the extensive experiments on two benchmark datasets, we achieve competitive detection accuracy, and more importantly, our approach is able to substantially reduce computational time and detect multiple activities in only 348ms for each untrimmed long video of THUMOS14 and ActivityNet.*

## 1. Introduction

Efficient temporal activity detection in untrimmed long videos is fundamental for intelligent video analytics including automatic categorizing, searching, indexing, segmentation, and retrieval of videos. This is a challenging problem as algorithms must (1) determine whether a specific activity occurs in an untrimmed video; (2) identify the temporal extent of each activity; and (3) maximize the detection accuracy within a given time or computational budget. In temporal activity detection, the most time consuming step is the execution of CNNs or hand-crafted feature extractors to every sliding window or proposal segment [4, 10, 39], typically taking, e.g., seconds to minutes to process one video in the THUMOS14 dataset [11]. Unfortunately, this rules out the practical use of these methods for applications that require real-time and large-scale video processing. Although

hardware solutions in some scenarios can help meet the constraints, it is equally important to establish a better understanding of how to achieve a maximal detection accuracy given the constraints on computation time and resources.

Recently, there is a fast growing interest in the research of temporal activity detection. Most existing work [18, 20, 27, 31, 39] hinges on a large set of features and classifiers that exhaustively run over every time step at multiple temporal scales. This sliding window approach is obviously computationally expensive for applications such as the ones running on the mobile or embedded devices. To avoid such exhaustive evaluations, a number of action proposal algorithms [4, 10, 24] have been proposed to produce a set of candidate temporal segments that are likely to contain a certain action. A separate classifier is then applied on these proposal segments for action classification. However, we argue that it is suboptimal to divide temporal activity detection into two disjointed steps of proposal and classification. Moreover, the large number of proposal segments (e.g., thousands of proposals per video) is still unsatisfying in term of computational efficiency.

In this paper, we address this problem by introducing a budget-aware and fully end-to-end framework that learns to optimally select a small number of video frames according to a time or computational budget to perform activity detection. We formalize our frame selection as a Markov decision process (MDP), and adopt a recurrent network to model the policy for selecting frames. We develop a policy gradient approach based on reinforcement learning to approximate the gradient of our non-decomposable and non-differentiable objective function. Figure 1 illustrates the detection process of our approach.

A similar problem is also recently studied in [38], where the goal is to efficiently localize actions by avoiding the need of processing most video frames. In that work, a recurrent attention model is learned to select a subset of video frames to interact with, and maintains high detection accuracy. Our work is different from [38] in: (1) unlike their binary model specifically trained for each action class, our approach is able to handle multiple classes; (2) rather than using a separate emission signal to identify foreground segments, we consider all predicted outputs as valid segments

\*Work done during an internship at NVIDIA Research.

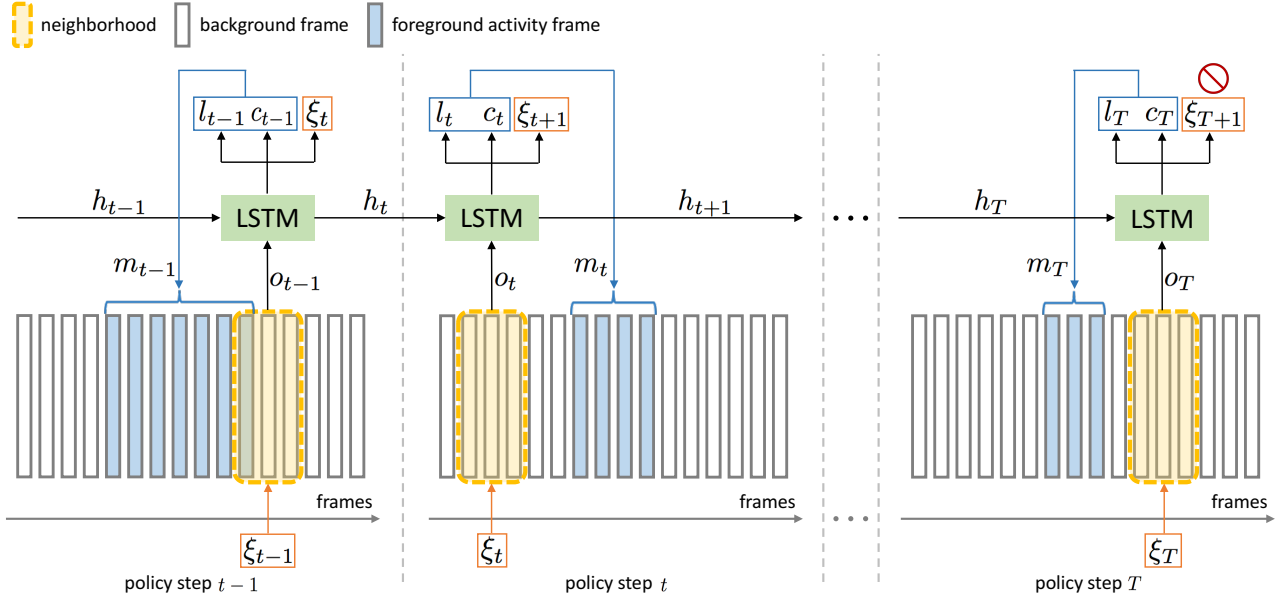


Figure 1. Given an untrimmed long video, at each step  $t$  the policy has access to the local observation  $o_t$  of a neighborhood centered around the current selected frame at  $\xi_t$ . For each step, the policy predicts a segment  $m_t$  and produces three outputs: the temporal location  $l_t$  (i.e., start and end) of the segment, the estimated class  $c_t$  of the segment, and the next frame to observe at  $\xi_{t+1}$ . The policy runs for  $T$  steps according to a specified time or computational budget, and then stops.

since we include the background as an additional class; (3) their reward function is designed to maximize true positives and minimize false positives, while our retrieval loss is directly defined on the mAP; and (4) instead of using two schemes (i.e., back-propagation for candidate detection and REINFORCE for prediction indicator and next observation) to train their learning agent, we employ a unified recurrent policy gradient to train the entire policy altogether.

Our main contributions of this paper are summarized as follows. First, we propose a budget-aware algorithm, which achieves competitive accuracy using only 348ms inference time for activity detection in each untrimmed minutes-long video. Second, we present a fully end-to-end policy based model with a single training phase to handle the activity classes in their entirety. Third, to our knowledge, we provide the first approach to directly optimize the mAP criteria (i.e., the final evaluation metric) in the objective function for activity detection.

## 2. Related Work

A large family of the research in video activity understanding is about activity classification, which provides useful tools for temporal activity detection, such as the iDT features [30] and the feature encoding with VLAD [12], the two-stream networks with two separate CNNs operating on the color and optical flow modalities [25], the dynamic image to compress temporal evolutions of a video into a single image [1], and the C3D using 3D-CNN to process short

video clips [29]. RNNs can be also applied on top of CNNs to model the temporal dynamics and handle variable-length video sequences [19].

Another active research line is the spatio-temporal action detection, which focuses on localizing action regions over consecutive video frames. A number of methods have been proposed, from the spatio-temporal proposals such as supervoxels [28], the frame-level object detection followed by a linking or tracking algorithm [7], to the recent video SSD approach [13]. However, these methods are mostly applied on short video snippets, in contrast, temporal activity detection targets at untrimmed videos that involve complex actions, objects and scenes evolving over long sequences. Therefore, efficient inference under budget is much in demand for the temporal activity detection task.

The problem of temporal activity detection is first described in [6] to temporally localize several simple actions such as “drinking” and “smoking” in untrimmed long videos. A majority of the existing approaches [18, 20, 27, 31, 39] focus on extracting various features to represent sliding windows and subsequently classifying them with SVMs trained on the multiple features. Alternative proposal based methods are proposed to generate action segments to replace the exhaustive sliding windows. A sparse learning based framework is presented in [10] to produce segment proposals with high recall. Escorcía et al. [4] introduce a proposal algorithm based on C3D and LSTM. Shou et al. [24] propose a 3D-CNN based multi-stage framework with three different networks for proposal, classifi-

cation and localization. A convolutional-de-convolutional network is further introduced in [23] to boost the precision for temporal boundaries of proposal segments. These proposal based detection methods are by nature stage-wised, and therefore are not end-to-end trainable. R-C3D is recently proposed in [37] to save computation through sharing convolutional features between proposal and classification pipelines. Richard and Gall [21] introduce a statistical language model based approach to perform action detection in a single step. Yeung et al. [38] present an end-to-end learning method to directly predict the temporal boundaries from raw videos. A detailed comparison between our approach and [38] is provided in Sec. 1. In the existing methods, there is no explicitly study about the trade-off between accuracy and efficiency under varying time constraints.

Research of budget-aware inference is receiving an increasing attention in computer vision. Recently, the budget-aware models have been explored for semantic segmentation in videos [16, 22, 33, 34], which have studied the structured prediction constrained to produce an output within a given time budget. This type of budget-aware structured prediction differs from anytime prediction, addressed, e.g., in [9, 14, 15], as the latter seeks to greedily improve the current prediction until the user stops the inference procedure. By contrast, in budget-aware inference, the prior knowledge of the budget constraint makes it possible to learn how to optimize a trade-off between accuracy and efficiency for the specified budget during training. While our approach proceeds along with this direction, we address a completely different problem with a distinct objective.

### 3. Problem Formulation

Given a video  $v$  and a set of activity labels  $\mathcal{L}$ , our goal is to predict for each frame a single label from  $\mathcal{L}$ . We call each temporal extent consisting of consecutive frames with the same label a semantic temporal segment. As stated in Sec. 1, given a limited time or computational budget, it is not feasible to process every single frame in a video. So we aim to detect and classify the foreground segments by only observing a small subset of video frames  $\mathbf{x} \in v$ .

Assuming limited access to the frames of  $v$ , the task of finding the optimal frame subset  $\mathbf{x}$  is inherently a sequential decision making task. Accordingly, we draw on ideas from reinforcement learning—an area that focuses on learning for sequential decision making problems. We aim to learn a policy  $\pi$ , parameterized by  $\theta$ , to sequentially select the frames from  $v$  and form the subset  $\mathbf{x}$ . Alongside the selection process,  $\pi$  outputs the current belief about the foreground segment and the associated class label. This sequential decision making process intuitively resembles how humans search activities in a video, i.e., iteratively refine our estimated temporal boundaries by sequentially choosing a few frames to observe.

Let  $\mathbb{G}$  denote the ground truth segments in  $v$  and  $\mathbb{M}^x$  be the set of estimated semantic temporal segments resulting from observing  $\mathbf{x}$ . We define the following deterministic indicator  $\mathbb{I}_{m,g}$  to identify if an estimated segment  $m \in \mathbb{M}^x$  is assigned to a ground truth segment  $g \in \mathbb{G}$ :

$$\mathbb{I}_{m,g} = \begin{cases} 1 & g = \arg \max_{g' \in \mathbb{G}} \alpha(m, g'), \text{ s.t. } \alpha > 0, \\ 0 & \text{otherwise,} \end{cases}$$

where  $\alpha$  is the intersection over union (IoU). Let  $c_m$  and  $c_g$  indicate the probability distribution and one-hot representation of the associated class labels for segments  $m$  and  $g$ , respectively. For a subset of selected frames  $\mathbf{x}$  and a set of predicted segments  $\mathbb{M}^x$ , our loss is defined as:

$$L_\theta = \sum_{m \in \mathbb{M}^x} \sum_{g \in \mathbb{G}} \mathbb{I}_{m,g} \left[ \lambda_c \Delta_{cls}(c_m, c_g) + \lambda_l \Delta_{loc}(l_m, l_g) \right] + \lambda_r \Delta_{ret}(\mathbb{M}^x, \mathbb{G}), \quad (1)$$

where  $\Delta_{cls}$  is the multi-class classification error,  $\Delta_{loc}$  is the localization error with  $l_m$  and  $l_g$  identifying the locations (i.e., start and end) of segments  $m$  and  $g$ , and  $\Delta_{ret}$  is the segment retrieval error. The most important property of the  $\Delta_{ret}$  is that while it encourages the model to detect all foreground segments, it also discourages the model from producing a large number of false positives.

We now explain how to formulate each individual error in Eq. (1). In contrast to using a binary classification loss as in [38], we employ a multi-class cross-entropy loss:

$$\Delta_{cls} = -c_g \log c_m. \quad (2)$$

Unlike [38] which penalizes the localization based on the absolute error, we believe the loss value should also depend on the duration of a segment, i.e., the same amount of absolute error should be treated differently for short and long intervals. Intuitively, this means that if the policy makes a small error for a short segment this error should be considered relatively large, otherwise the algorithm would ignore small segments. With this intention, we define  $\Delta_{loc}$  as:

$$\Delta_{loc}(l_m, l_g) = \zeta(g) \times \|(m_s, m_e), (g_s, g_e)\|, \quad (3)$$

where  $\zeta(g)$  is a scaling factor which depends on the length of segment  $g$ ,  $\|\cdot\|$  is the distance between two segments,  $m_s$  and  $m_e$  are the start and end of segment  $m$ , similar for segment  $g$ . To define the segment retrieval loss  $\Delta_{ret}(\mathbb{M}^x, \mathbb{G})$ , we use the mAP criteria, where mean is over different class labels, and AP for each individual class is defined as:

$$\text{AP}(\mathbb{M}^x, \mathbb{G}) = \sum_j \text{Prec}(\mathbb{M}^x(j), \mathbb{G}) \times \Delta_{\text{Recall}}, \quad (4)$$

where  $\mathbb{M}^x(j)$  is the subset of  $\mathbb{M}^x$  till the  $j$ th segment ranked by the overlap with ground truth,  $\text{Prec}(\cdot)$  is the precision of

detection, and  $\Delta_{\text{Recall}}$  is the change of recall from previous subset. Given a training set of  $N$  videos  $\{v_1, \dots, v_N\}$ , our goal is to find  $\theta$  that minimizes the following:

$$\theta^* = \arg \min_{\theta} [\mathbb{E}(L_{\theta}) \approx \frac{1}{N} \sum_{n=1}^N L_{\theta}(\mathbb{M}_n^x, \mathbb{G}_n)]. \quad (5)$$

Unfortunately, standard back-propagation is not applicable to learn the parameters in Eq. (5), as the objective function in Eq. (1) includes the non-differentiable components. This is mainly due to the non-decomposable AP defined in Eq. (4), as well as the sequential decision making process in selecting frames. In order to solve this difficulty, we reformulate our problem as a reinforcement learning problem, which allows us to define an equivalent reward function to the original objective function.

## 4. Recurrent Policy Network

In this section, we describe our proposed representation for the policy  $\pi$ , and present the approach for learning the parameters  $\theta$  by drawing on the recurrent policy gradient estimation technique.

### 4.1. Policy Representation

Our agent of activity detection makes a sequence of predictions based on the local information obtained around the most recent observed frame. At each step of this sequential decision making process, the policy produces three outputs, which includes the estimate of start and end of the current potential temporal segment, the prediction of the class label associated with the segment, and the next frame to observe. Unlike the binary model used in [38], our approach enables us to define a multi-class classifier, which means that we only need to train a single policy rather than training multiple different policies. Note that this also allows us to avoid the binary prediction indicator signal used in [38], since we can directly discard those segments predicted with the background label.

It is also important to point out that due to the local observation at each step, the policy has no access to the global state (i.e., the entire video). This resembles the partially observable Markov decision process (POMDP), where it is assumed that despite the existence of a global state, for practical reasons an agent does not have a full observation of the global state. Restricting the observation of the policy to a short interval around the current frame is to limit the number of feature extractions on video frames by CNN so as to reduce the computation time for each step. Additionally, it is impractical to include features from the entire video in every single observation of the agent.

We adopt the recurrent policy gradient approach [35] to maintain an approximate belief of the current state  $s_t$  by using a recurrent network. More specifically, at each step the

agent updates its belief of the world through the local partial observation. We exploit LSTM as the recurrent network due to its strong capacity to memorize the information from previous observations as well as the decisions made by the policy. As shown in [8, 16, 17], LSTM have been successfully applied to these POMDP problems and provide close to optimal decisions.

Particularly, suppose at step  $t$  the current frame is  $i$ , the policy  $\pi$  makes a decision based on (1) the local information of a neighborhood  $\mathcal{N}_i$  centered around  $i$  and (2) the history of previous observations. We capture the local information through an observation feature  $o_t = [\psi(\mathcal{N}_i), \phi(\mathcal{N}_i), \xi_t]$ , where  $\psi(\mathcal{N}_i)$  is an indicator vector that identifies whether each frame in  $\mathcal{N}_i$  has been previously selected,  $\phi(\mathcal{N}_j)$  is the average of per-class confidence predicted in  $\mathcal{N}_j$ , and  $\xi_t \in [0, 1]$  is the normalized location of the current frame at step  $t$  (e.g., the middle frame has value 0.5). The inclusion of  $\xi_t$  is helpful in encouraging the policy to cover broader video extent. During our experiments, we find that excluding  $\xi_t$  results in a considerable number of over-selection of frames. Note that for  $\phi$ , we compute the averaged confidence of estimated segments, which share the frames in  $\mathcal{N}_i$ . As for the history of the decision makings, we use the hidden state  $h_{t-1}$  of LSTM to maintain the context of previous observations up to step  $t$ .

To summarize, the global state at step  $t$  is approximated by the internal state  $h_t$  of LSTM, which depends on the current observation  $o_t$  and the previous state  $h_{t-1}$ . Given  $h_t$  the outputs of the policy  $\pi$  are  $\nu_t = [l_t, c_t, \xi_{t+1}]$ : (1) the location  $l_t$  of an estimated temporal segment, (2) the probability distribution over activity class labels  $c_t$ , and (3) the location of the next observation  $\xi_{t+1}$ . Note that our formulation allows the policy to perform both forward and backward selections. In order to further improve the exploration at training phase, instead of directly using  $\xi_{t+1}$ , the next selected location is sampled from a Gaussian distribution with a mean equal to  $\xi_{t+1}$  and a fixed variance (0.18 used in our experiments).

### 4.2. Policy Learning

Our goal of policy learning is to jointly optimize the parameters of  $\pi$  by minimizing the loss of a sequence of policy actions as defined in Eq. (1). These actions are taken from the initial state  $s_0$ , when no frames are selected, until the final state  $s_T$ , where  $T$  is the number of steps specified according to a time or computational budget.

The main difficulty in policy learning is that the estimated temporal segments  $\mathbb{M}^x$  for each video are computed through a sequence of decisions made by the policy. This results in a non-decomposable and non-differentiable objective function. Moreover, a decision that the policy makes at any step depends on the history of decisions that the policy has made in previous steps, and also influences the deci-

sions available to the policy in the future. This is a long-standing problem in the research of reinforcement learning. Among the potential algorithms for addressing similar POMDP problems [2, 3, 35, 36], we adopt the recurrent policy gradient approach [35], which provides better theoretical bounds on the learning objective, to approximate the gradients of our non-decomposable and non-differentiable objective function, so that the policy can be efficiently learned with stochastic gradient descent.

To follow the general reinforcement learning formulation, let  $r$  be the immediate reward associated with a state  $s_t$ . Since  $s_t \approx h_t$  in our policy, we define  $r$  as:

$$r(h_t) = L_\theta(\mathbb{M}_{t-1}^x, \mathbb{G}) - L_\theta(\mathbb{M}_t^x, \mathbb{G}), \quad (6)$$

where  $L_\theta$  is the loss associated with a set of estimated temporal segments as defined in Eq. (1). Intuitively,  $r(h_t)$  states that the policy earns an immediate reward equal to the decrease in the temporal segmentation error achieved by selecting an observed frame, or pays a penalty if the temporal segmentation error increases. Let  $R(H_t)$  be the discounted accumulated reward starting from the state  $s_t$  and continuing the policy up to the final state  $s_T$ :

$$R(H_t) = \sum_{t'=t}^T \tau^{t'-t} r(h_{t'}), \quad (7)$$

where  $H_t = \{h_t, \dots, h_T\}$  represents the history of hidden states in LSTM, and  $\tau \in (0, 1)$  is the discount factor.  $H_0$  can be interpreted as the trajectory of observations for a sample run of the policy from the initial state. For notational simplicity, we use  $H$  for  $H_0$  in the rest of this paper. The goal of policy learning is transformed to find the parameters  $\theta^*$  to maximize  $J(\theta)$  which is defined as:

$$J(\theta) = E[R(H)] = \int p(H|\theta) R_\theta(H) dH, \quad (8)$$

where  $p(H|\theta)$  is the probability of observing a sequence of hidden states  $H$ , given a policy  $\pi$  defined by the parameters  $\theta$ . It can be shown that maximizing  $J(\theta)$  implicitly minimizes  $L_\theta$  along the trajectory of policy executions.

We now derive how to compute the gradient with respect to the policy parameters  $\nabla_\theta J$ , which is given by:

$$\nabla_\theta J = \int [\nabla_\theta p(H|\theta) R_\theta(H) + p(H|\theta) \nabla_\theta R_\theta(H)] dH. \quad (9)$$

Note that given the sequence of hidden states  $H$ , which determines the history of selected frames, the reward function does not depend on the policy parameters, yielding  $\nabla_\theta R_\theta(H) = 0$ . To further simplify Eq. (9), we need to define  $\nabla_\theta p(H|\theta)$ , so we first factorize  $p(H|\theta)$  as:

$$p(H|\theta) = p(h_0) \prod_{t=1}^T p(h_t|h_{t-1}) \pi(\nu_t|h_{t-1}, o_t), \quad (10)$$

where the same notation  $\pi$  is used to denote the output of the policy. From Eq. (10) we have:

$$\log p(H|\theta) = \text{const} + \sum_{t=1}^T \log \pi(\nu_t|h_{t-1}, o_t), \quad (11)$$

where the first term is a sum over the log of  $p(h_t|h_{t-1})$ , which is const with respect to  $\theta$ . Eq. (11) therefore results in the following gradient:

$$\nabla_\theta \log p(H|\theta) = \sum_{t=1}^T \nabla_\theta \log \pi(\nu_t|h_{t-1}, o_t). \quad (12)$$

It is common to use the Monte-Carlo integration to approximate the integration over the probability of observing a sequence of hidden states. Specifically, the approximate gradient is computed by running the current policy on  $N$  training videos to generate  $N$  trajectories. Combining Eqs. (9-12), we can obtain the following approximate gradient:

$$\nabla_\theta J \approx \frac{1}{N} \sum_{n=1}^N \sum_{t=1}^T [\nabla_\theta \log \pi(\nu_t|h_{t-1}^n, o_t^n) R_\theta(h_t^n)]. \quad (13)$$

Since the policy gradient methods usually suffer from the high variance of gradient estimates, we follow the common practice used in [36] to subtract a bias from the expected reward  $R$ . However, rather than taking a constant bias, we set the bias value to be the reward obtained from a random selection policy.

## 5. Experiments

In this section, we extensively evaluate our approach on the two benchmark datasets: THUMOS14 [11] and ActivityNet [5]. Experimental results demonstrate that our approach is able to substantially reduce computational time, and meanwhile provides competitive detection accuracy under varying budgets. In the section of appendix, we explain how to calculate the approximate computational time of different methods.

### 5.1. Implementation Details

We use the pre-trained VGG16 [26] on ImageNet as our backbone CNN, and fine-tune the network on the activity classes of each dataset. We employ the fc7 layer of VGG16 as the per-frame feature descriptor. Our policy is based on a two-layer LSTM, and each layer has 1024 hidden units. If not otherwise specified, our policy takes  $T = 6$  steps, which we believe are efficient enough to meet a reasonable budget constraint. We empirically set the weights in our loss function as  $\lambda_c = \lambda_l = 1.0$  and  $\lambda_r = 0.5$ . We set the batch size to 128 and train the models for 100 epochs using the Adam optimizer with default parameters. We implement our models in TensorFlow and perform experiments on a single NVIDIA Tesla P100 GPU.

Method	0.3	0.4	0.5	0.6	0.7
CNN with NMS	12.6	9.7	6.1	4.1	2.4
CNN <sub>dif</sub> with NMS	15.9	13.1	10.2	5.4	3.8
LSTM with NMS	12.8	11.3	9.4	6.4	3.9
LSTM <sub>dif</sub> with NMS	18.4	19.2	15.1	9.7	4.1
Ours <sub>bas</sub>	34.1	24.2	17.4	10.6	6.2
Ours <sub>dif</sub>	37.6	26.7	20.9	10.9	6.6
Ours <sub>reg</sub> , $\kappa = 5$	38.3	27.5	21.1	11.2	7.1
Ours <sub>reg</sub> , $\kappa = 10$	38.4	28.9	22.4	11.4	7.0
Ours <sub>reg</sub> , $\kappa = 20$	38.7	28.5	22.5	11.8	7.1

Table 1. Comparison of the detection accuracy (mAP) of base models and variations of our model under different IoU thresholds  $\alpha$  on the THUMOS14 dataset.

## 5.2. Baselines and Variations of Our Model

To provide a better insight, we first conduct a study of the different possible configurations of our model and baseline methods. We define the following two important baselines, each of them outputs a class label for a single frame including the background class, followed by a non-maximum suppression (NMS) post-processing to aggregate the class probabilities of single frames.

- **Single frame CNN with NMS:** VGG16 is fine-tuned on the single frames of each dataset and used to perform per-frame classification.
- **Single frame LSTM with NMS:** We train a one-layer LSTM with a 512-dimensional hidden state on top of the  $\text{fc7}$  layer of VGG16, and a prediction is made for each single frame.

We can improve our base model mainly in two ways and define multiple variations of our model as follows.

- **Ours<sub>bas</sub>** is the base model defined in Sec. 4.1.
- **Ours<sub>dif</sub>** provides the simple pixel-level frame difference between consecutive frames in the neighborhood as an additional feature to roughly capture motion cues. Although in theory, we can incorporate optical flow based features, given the fact that optical flow is computationally expensive, and the motivation of this work is for efficient inference, we believe that the pixel-level frame subtraction is a reasonable compromise. We use early-fusion to concatenate RGB channels of the original frame and the frame difference as a composite input to VGG16.
- **Ours<sub>reg</sub>** performs a simple post-processing to refine the policy output. We train a simple linear regressor to refine the boundaries of detected temporal segments. The input features for this regressor are the current temporal extend of a segment, and the  $\kappa$  uniformly sampled frames along with their pixel-level frame differences within this segment.

## 5.3. Results on THUMOS14

There are 20 action classes of sports in the temporal action detection task of THUMOS14 [11]. We follow the standard experimental setting, i.e., 2,755 trimmed training videos and 1,010 untrimmed validation videos are used for training our model, and 213 untrimmed testing videos for evaluation. We provide mAP under different IoU thresholds  $\alpha \in [0.3, 0.7]$ .

We first present the ablation experiments to understand the contribution of each individual component in our model. As expected and shown in Table 1, providing the additional simple frame difference to capture the coarse motion cues improves the accuracy of all baselines and our models. Similarly, the baseline recurrent models with LSTM are found to produce better results than CNN. We believe this is mainly because of the larger temporal context that the recurrent network can access. All of our ablation models significantly outperform the baselines, quantifying the contributions of our proposed approach. In particular, our results are produced by only observing 6 policy selected frames, far more efficient than the baselines that have to go through all video frames densely.

It is interesting to observe that the simple linear regression based post-processing with  $\kappa$  uniformly sampled frames from the policy estimated segments helps in refining the temporal boundaries. We conjecture that this is due to the fact that our policy is allowed to observe frames in a temporally inconsistent way (i.e., selecting frames in a mixed forward and backward fashion). Thus, LSTM tends to smooth out the features to some extent during this process. We hypothesize that observing the  $\kappa$  sampled frames along the estimated temporal segment in the simple post-processing provides a complementary high-level and temporally consistent description to the averaged latent representation that lacks temporal consistency in the policy. We also evaluate the impact of the number of sampled frames  $\kappa$  to the regression. As shown in Table 1, we only observe marginal gains when sampling over 10 frames, which also implies that our policy has already learned to select fairly representative frames to perform the detection.

We then compare with the state-of-the-art methods in Table 2. Our approach achieves competitive detection accuracy under various IoU thresholds, and more importantly, we perform the detection in only 348ms on average for each untrimmed long video. This is orders of magnitude faster than most other competing algorithms relying on expensive sliding windows or segment proposals, which contradicts our primary goal of reducing the overall inference time. While R-C3D produces superior detection accuracy on this dataset, we significantly outperform R-C3D on ActivityNet (see Table 4), indicating the advantage of our approach to handle more complex activities. We specifically compare the per-class breakdown AP of our model and the

Method	Time	$\alpha = 0.3$	$\alpha = 0.4$	$\alpha = 0.5$	$\alpha = 0.6$	$\alpha = 0.7$
LEAR14 [20]	> 108s	28.8	21.8	15.0	8.5	3.2
CUHK14 [31]	> 108s	14.6	12.1	8.5	4.7	1.5
Pyramid of Score Distribution [39]	> 108s	33.6	26.1	18.8	-	-
Fast Temporal Proposals [10]	108s	-	-	13.5	-	-
S-CNN [24]	92s	36.3	28.7	19.0	10.3	5.3
CDC [23]	92s	40.1	29.4	23.3	13.1	7.9
DAPs [4]	41s	-	-	13.9	-	-
Statistical Language Model [21]	17s	30.0	23.2	15.2	-	-
R-C3D [37]	10s	44.8	35.6	28.9	-	-
Frame Glimpse [38]	5s	36.0	26.4	17.1	-	-
Ours	348ms	38.4	28.9	22.4	11.4	7.0

Table 2. Comparison of our approach and the state-of-the-art methods in the approximate computational time to process each video and the detection accuracy (mAP) under different IoU thresholds  $\alpha$  on the THUMOS14 dataset.

Class	[38]	Ours	Class	[38]	Ours
Base. Pitch	14.6	19.5	Hamm. Throw	28.9	25.3
Basket. Dunk	6.3	13.1	High Jump	33.3	41.4
Billiards	9.4	8.3	Javelin Throw	20.4	29.1
Clean & Jerk	42.8	48.7	Long Jump	39.0	46.7
Cliff Diving	15.6	22.4	Pole Vault	16.3	26.3
Cricket Bowl.	10.8	19.8	Shotput	16.6	21.8
Cricket Shot	3.5	11.3	Socc. Penalty	8.3	6.7
Diving	10.8	17.4	Tennis Swing	5.6	11.8
Frisb. Catch	10.4	9.3	Throw Discus	29.5	41.2
Golf Swing	13.8	22.8	Volley. Spike	5.2	4.8
mAP				17.1	22.4

Table 3. Comparison of the per-class breakdown AP at IoU of  $\alpha = 0.5$  on the THUMOS14 dataset.

frame glimpse method [38], which also exhibits efficient inferencing capability for each binary detection. As shown in Table 3, our approach largely outperforms [38] in 15 out of 20 classes, and 5.3 in overall mAP. Notably, our method is a unified model to handle all classes, while [38] is a binary model that needs to be trained for each specific class of the 20 actions, and therefore we need to run their model 20 times to detect the whole classes.

We also provide the in-depth analysis of the computational costs of our approach. Figure 2 shows the percentage of time for each major algorithm step and computation component. Our policy is efficient to run, only taking 9.4% of the time. The feature extraction that involves applying CNN to multiple frames dominates the computations, consuming 80.1% of the time, which highlights the importance of effective frame selection to reduce dense feature extractions. Moreover, it only takes 2.9% to compute the frame differ-

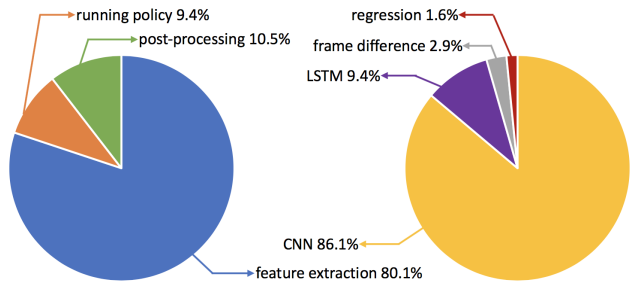


Figure 2. Analysis of computational time of our approach: percentage of time spent on each major algorithm step (left) and computation component (right) to perform activity detection.

ence, which can provide coarse but useful motion cues. In the section of appendix, we present the illustration of the learned policy for frame selection as well as the examples of our model’s predictions.

## 5.4. Results on ActivityNet

ActivityNet [5] consists of around 10K training videos and 4K validation videos in 200 activity classes with 1.54 activity instances on average in each video. Since having no access to the annotations of testing set, we use the training set for training and the validation set for testing. Compared with THUMOS14, ActivityNet involves high-level semantics with complex actions, objects and scenes in videos, and is a much larger dataset in terms of both number of activities and amount of videos.

With this large-scale dataset, we first evaluate our model for different numbers of steps the policy can take, which corresponds to the different time or computational budgets the detection system can afford. As shown in Table 5, when we increase the policy steps from 6 to 14 by raising the time or computational budgets, the detection accuracy is improved by 0.5 mAP under  $\alpha = 0.5$ , but without significant difference for more strict thresholds.

Method	Time	$\alpha = 0.5$	$\alpha = 0.75$	$\alpha = 0.95$	Ave-mAP
UTS16 [32]	> 930s	45.1	4.1	0.0	16.4
CDC [23]	> 930s	45.3	26.0	0.2	23.8
UPC16 [18]	11s	22.5	-	-	-
OBU16 [27]	10s	22.7	10.8	0.3	11.3
R-C3D [37]	6s	26.8	-	-	12.7
Ours	348ms	41.9	22.6	0.1	21.5

Table 4. Comparison of our approach and the state-of-the-art methods in the approximate computational time to process each video and the detection accuracy (mAP) under different IoU thresholds  $\alpha$  on the ActivityNet dataset.

Steps	Time	$\alpha = 0.5$	$\alpha = 0.75$	$\alpha = 0.95$
$T = 6$	348ms	41.9	22.6	0.1 (0.07)
$T = 10$	556ms	42.1	22.1	0.1 (0.07)
$T = 14$	764ms	42.4	22.5	0.1 (0.08)

Table 5. Comparison of different policy steps specified for our approach in the detection accuracy (mAP) under different IoU thresholds  $\alpha$  on the ActivityNet dataset.

Class	[38]	Ours	Class	[38]	Ours
Archery	5.2	13.7	Long Jump	56.8	48.7
Bowling	52.2	52.4	Mtn. Clim.	53.0	52.4
Bungee	48.9	46.3	Paintball	12.5	24.9
Cricket	38.4	39.1	Play. Kick.	60.8	61.2
Curling	30.1	32.3	Play. Volley.	40.2	39.2
Discus Throw	17.6	21.8	Pole Vault	35.5	40.2
Dodgeball	61.3	60.2	Shot Put	50.9	51.4
Doing Moto.	46.2	47.3	Skateboard.	34.4	32.7
Ham. Throw	13.7	18.8	Start Fire	38.4	40.1
High Jump	21.9	27.4	Triple Jump	16.1	22.7
Javelin Throw	35.7	40.1			
mAP				36.7	38.7

Table 6. Comparison of the per-class breakdown AP at IoU of  $\alpha = 0.5$  on the sports subset of the ActivityNet dataset.

Finally, we compare our approach with the state-of-the-art methods in Table 4. Similar to the results on THU-MOS14, our approach substantially reduces the inference time by orders of magnitude. While CDC provides very competitive accuracy, it relies on the detection results of UTS16, i.e., it is mainly used to refine the predicted temporal segments of UTS16. If directly applying CDC on raw videos, the accuracy will drop to around 15 mAP at  $\alpha = 0.5$ . UTS16 is sliding window based, and requires extensive feature extractions including iDT, C3D, and VLAD encoded deep features of ResNet152 and InceptionV3, which are considerably expensive for inference. We achieve significant improvement over the most recent state-of-the-art method R-C3D, demonstrating the superiority of our approach to model the more complex activities.

Class	[38]	Ours	Class	[38]	Ours
Attend Conf.	56.5	53.8	Phoning	52.1	46.7
Sch. Security	33.9	36.1	Pump. Gas	34.0	49.3
Buy Fast Food	45.8	48.2	Setup Comp.	30.3	35.1
Clean Laptop	35.8	38.3	Sharp. Knife	35.2	38.3
Make. Copies	41.7	39.5	Sort Books	16.7	33.7
Org. Boxes	19.1	24.5	Using Comp.	50.2	47.3
Org. Cabin.	43.7	46.2	Using ATM	64.9	50.6
Packing	39.1	38.3			
mAP				39.9	41.7

Table 7. Comparison of the per-class breakdown AP at IoU of  $\alpha = 0.5$  on the work subset of the ActivityNet dataset.

Since the frame glimpse method [38] is a binary model and their detection results on the entire 200 classes of this dataset are not provided, we train our policy on the same two subsets (i.e., sports and work) as [38] for a fair comparison. Table 6 and Table 7 show that our approach performs better than [38] in 15 out of 21 classes on the sports subset, and 9 out of 15 classes on the work subset. Overall, we outperform [38] by 2.0 and 1.8 in term of mAP on the sports and the work subsets, respectively.

## Conclusion

In this paper, we have presented a fully end-to-end approach for the challenging problem of efficient temporal activity detection. We formulate a budget-aware inference for this problem to optimally select a small subset of video frames. We formalize the frame selection process within the MDP framework and propose the LSTM based policy model to handle the whole activity classes with a single training phase. A policy gradient is further developed to approximate the gradient of our non-decomposable and non-differentiable objective. Experimental results on the two benchmark datasets demonstrate that our approach can bring substantial time saving and maintain competitive detection accuracy. This provides an efficient solution for many applications that require tight runtime constraints and limited on-device computations.

## References

- [1] H. Bilen, B. Fernando, E. Gavves, A. Vedaldi, and S. Gould. Dynamic image networks for action recognition. In *CVPR*, 2016. 2
- [2] S. Cho, S. Cho, and K. C. Yow. A robust time series prediction model using POMDP and data analysis. *Journal of Advances in Information Technology*, 2017. 5
- [3] M. Egorov, Z. N. Sunberg, E. Balaban, T. A. Wheeler, J. K. Gupta, and M. J. Kochenderfer. POMDPs.jl: A framework for sequential decision making under uncertainty. *JMLR*, 2017. 5
- [4] V. Escorcia, F. Heilbron, J. Niebles, and B. Ghanem. DAPs: Deep action proposals for action understanding. In *ECCV*, 2016. 1, 2, 7, 10
- [5] B. G. Fabian Caba Heilbron, Victor Escorcia and J. C. Niebles. ActivityNet: A large-scale video benchmark for human activity understanding. In *CVPR*, 2015. 5, 7
- [6] A. Gaidon, Z. Harchaoui, and C. Schmid. Temporal localization of actions with actoms. *TPAMI*, 2013. 2
- [7] G. Gkioxari and J. Malik. Finding action tubes. In *CVPR*, 2015. 2
- [8] K. Gregor, I. Danihelka, A. Graves, and D. Wierstra. DRAW: A recurrent neural network for image generation. In *ICML*, 2015. 4
- [9] A. Grubb, D. Munoz, J. A. Bagnell, and M. Hebert. Speed-Machines: Anytime structured prediction. *arXiv:1312.0579*, 2013. 3
- [10] F. Heilbron, J. Niebles, and B. Ghanem. Fast temporal activity proposals for efficient detection of human actions in untrimmed videos. In *CVPR*, 2016. 1, 2, 7, 10
- [11] H. Idrees, A. R. Zamir, Y.-G. Jiang, A. Gorban, I. Laptev, R. Sukthankar, and M. Shah. The THUMOS challenge on action recognition for videos “in the wild”. *CVIU*, 2017. 1, 5, 6
- [12] H. Jegou, M. Douze, C. Schmid, and P. Perez. Aggregating local descriptors into a compact image representation. In *CVPR*, 2010. 2
- [13] V. Kalogeiton, P. Weinzaepfel, V. Ferrari, and C. Schmid. Action tubelet detector for spatio-temporal action localization. In *ICCV*, 2017. 2
- [14] S. Karayev, M. Fritz, and T. Darrell. Anytime recognition of objects and scenes. In *CVPR*, 2014. 3
- [15] B. Liu and X. He. Learning dynamic hierarchical models for anytime scene labeling. In *ECCV*, 2016. 3
- [16] B. Mahasseni, S. Todorovic, and A. Fern. Budget-aware deep semantic video segmentation. In *CVPR*, 2017. 3, 4
- [17] V. Mnih, N. Heess, A. Graves, and K. Kavukcuoglu. Recurrent models of visual attention. In *NIPS*, 2014. 4
- [18] A. Montes, A. Salvador, S. Pascual, and X. Giro. Temporal activity detection in untrimmed videos with recurrent neural networks. In *NIPS Workshop*, 2016. 1, 2, 8, 11
- [19] J. Ng, M. Hausknecht, S. Vijayanarasimhan, O. Vinyals, R. Monga, and G. Toderici. Beyond short snippets: Deep networks for video classification. In *CVPR*, 2015. 2
- [20] D. Oneata, J. Verbeek, and C. Schmid. The LEAR submission at THUMOS 2014. In *ECCV THUMOS Workshop*, 2014. 1, 2, 7, 10
- [21] A. Richard and J. Gall. Temporal action detection using a statistical language model. In *CVPR*, 2016. 3, 7, 10
- [22] G. Roig, X. Boix, R. D. Nijs, S. Ramos, K. Kuhlentz, and L. V. Gool. Active MAP inference in CRFs for efficient semantic segmentation. In *ICCV*, 2013. 3
- [23] Z. Shou, J. Chan, A. Zareian, K. Miyazawa, and S.-F. Chang. CDC: convolutional-de-convolutional networks for precise temporal action localization in untrimmed videos. In *CVPR*, 2017. 3, 7, 8, 10, 11
- [24] Z. Shou, D. Wang, and S.-F. Chang. Temporal action localization in untrimmed videos via multi-stage CNNs. In *CVPR*, 2016. 1, 2, 7, 10
- [25] K. Simonyan and A. Zisserman. Two-stream convolutional networks for action recognition in videos. In *NIPS*, 2014. 2
- [26] K. Simonyan and A. Zisserman. Very deep convolutional networks for large-scale image recognition. In *ICLR*, 2015. 5
- [27] G. Singh and F. Cuzzolin. Untrimmed video classification for activity detection: Submission to ActivityNet challenge. In *CVPR ActivityNet Workshop*, 2016. 1, 2, 8, 11
- [28] K. Soomro, H. Idrees, and M. Shah. Predicting the where and what of actors and actions through online action localization. In *CVPR*, 2016. 2
- [29] D. Tran, L. Bourdev, R. Fergus, L. Torresani, and M. Paluri. C3D: Generic features for video analysis. In *ICCV*, 2015. 2
- [30] H. Wang, D. Oneata, J. Verbeek, and C. Schmid. A robust and efficient video representation for action recognition. *IJCV*, 2015. 2
- [31] L. Wang, Y. Qiao, and X. Tang. Action recognition and detection by combining motion and appearance features. In *ECCV THUMOS Workshop*, 2014. 1, 2, 7, 10
- [32] R. Wang and D. Tao. UTS at ActivityNet 2016. In *CVPR Workshop*, 2016. 8, 11
- [33] D. Weiss, B. Sapp, and B. Taskar. Dynamic structured model selection. In *ICCV*, 2013. 3
- [34] D. J. Weiss and B. Taskar. Learning adaptive value of information for structured prediction. In *NIPS*, 2013. 3
- [35] D. Wierstra, A. Förster, J. Peters, and J. Schmidhuber. Recurrent policy gradients. *Logic Journal of the IGPL*, 2010. 4, 5
- [36] R. J. Williams. Simple statistical gradient-following algorithms for connectionist reinforcement learning. *Machine Learning*, 1992. 5
- [37] H. Xu, A. Das, and K. Saenko. R-C3D: Region convolutional 3D network for temporal activity detection. In *ICCV*, 2017. 3, 7, 8, 10, 11
- [38] S. Yeung, O. Russakovsky, G. Mori, and L. Fei-Fei. End-to-end learning of action detection from frame glimpses in videos. In *CVPR*, 2016. 1, 3, 4, 7, 8, 10, 11
- [39] J. Yuan, B. Ni, X. Yang, and A. Kassim. Temporal action localization with pyramid of score distribution features. In *CVPR*, 2016. 1, 2, 7, 10

In this appendix, we summarize how to calculate the approximate computation time of different methods in Sec. A. Sec. B illustrates the frame selection and prediction process of our approach. Sec. C demonstrates the examples of detected activities by our model.

## A. Estimation of Computation Time

It is challenging to decide the precise computation time of the different methods due to (1) lack of computational information in the literature, and (2) multiple complex stages involved. We adopt the following strategies to estimate the approximate computation time for them: (1) directly use the speed or time if it is reported in related papers; (2) use the speed or time of our components (e.g., CNN and LSTM) to infer others; (3) use the processing bottleneck which dominates the computational costs (e.g., extraction of hand-crafted features) to approximate the overall time.

### A.1. THUMOS14

There are 20 action classes and 1574 videos in the testing set of THUMOS14. Each video has 5507 frames on average.

- **Ours** is provided in the analysis of computational costs in the paper. The detailed computation time of each component is: forward pass of VGG16 is 3.0ms for each frame on the GPU; execution time of 2-layer LSTM at each step is 5.4ms on the GPU; pixel-level frame difference is 0.1ms per frame on the CPU; linear regression is 5.5ms on the CPU. We use 6 steps to run our policy for each video, 15 frames as the neighborhood of each selected frame, and 10 uniformly sampled frames for regression. So the overall computation time for each video is:  $(0.1 \times 15 \times 6) + (3.0 \times 15 \times 6) + (5.4 \times 6) + (0.1 \times 10) + (3.0 \times 10) + 5.5 \approx 348\text{ms}$ .
- **Frame Glimpse** [38] downsamples videos by 5 (i.e., to 5fps) for this dataset, and observes 2% (or less) of video frames for inference. Since it is a binary model, we need to train and run 20 models to detect all classes of this dataset. Based on the time of our approach, we can infer the computation time of each component in [38]: forward time of VGG16 is 3.0ms for each frame on the GPU; execution time of 3-layer LSTM at each observation is 8.2ms on the GPU. So the average computation time to detect the whole classes for each videos is:  $5507 \div 5 \times 0.02 \times (3.0 + 8.2) \times 20 \approx 5\text{s}$ .
- **R-C3D** [37] runs at 569fps on an NVIDIA Titan X Maxwell GPU and 1030fps on an NVIDIA Titan X Pascal GPU. So the average computation time to predict each video is:  $5507 \div 569 \approx 10\text{s}$  on Titan X Maxwell, and  $5507 \div 1030 \approx 5\text{s}$  on Titan X Pascal.
- **Statistical Language Model** [21] uses 7.5h on the CPU with eight 1.2GHz cores for inference on this dataset. So the average computation time for each video is:  $7.5 \times 60 \times 60 \div 1574 \approx 17\text{s}$ .
- **DAPs** [4] integrates C3D and LSTM, and runs at 134.1fps on the GPU. So the average computation time to predict each video is:  $5507 \div 134.1 \approx 41\text{s}$ .
- **S-CNN** [24] employs the proposal and localization networks for inference, and runs at 60fps on the GPU. So the average computation time for each videos is:  $5507 \div 60 \approx 92\text{s}$ .
- **CDC** [23] alone runs at 500fps on the GPU to refine predicted temporal boundaries. However, on this dataset, it relies on the proposals generated by S-CNN [24], which dominates the computational costs. So the overall computation time including segment proposal and prediction refinement for each video can be approximated by that of S-CNN: 92s.
- **Fast Temporal Proposal** [10] downsamples videos by 5 and runs at 10.2fps on the CPU. So the average computation time for each video is:  $5507 \div 5 \div 10.2 \approx 108\text{s}$ .
- **Pyramid of Score Distribution** [39] uses a sliding window strategy, and requires time-consuming feature extraction, e.g., 21d to extract the iDT features on the CPU, 20h for feature encoding on the CPU, etc. So the average computation time to predict each video is much longer than the proposal based method [10]:  $> 108\text{s}$ .
- **CUHK14** [31] is also a sliding window based approach. It extracts deep features by AlexNet, and iDT features running at 3.5fps on the CPU. Additional computations include FV encoding of iDT features and SVM classification. So the average computation time to process each video is also much longer than the proposal based method [10]:  $> 108\text{s}$ .
- **LEAR14** [20] is also based on sliding windows with computationally expensive feature extractions: SIFT, iDT, color features, FV encoding, deep features by AlexNet, as well as acoustic features such as MFCC and ASR. So the average computation time to predict each video is also much longer than the proposal based method [10]:  $> 108\text{s}$ .

### A.2. ActivityNet

There are 200 activity classes and 4926 videos in the validation set of ActivityNet. Each video has 3254 frames on average.

- **Ours** is independent of the video length, but is determined by the number of steps to run our policy. We take the same processing as for THUMOS14 to per-

form activity detection on this dataset. So the overall computation time to predict each video is the same:  
 $(0.1 \times 15 \times 6) + (3.0 \times 15 \times 6) + (5.4 \times 6) + (0.1 \times 10) + (3.0 \times 10) + 5.5 \approx 348\text{ms}$ .

- **Frame Glimpse** [38] downsamples videos by 25 (i.e., to 1fps) for this dataset, and observes 2% (or less) of video frames for inference. Similarly, we need to train and run 200 models to detect the whole classes of this dataset. So the average computation time to detect the entire classes for each video is:  
 $3254 \div 25 \times 0.02 \times (3.0 + 8.2) \times 200 \approx 6\text{s}$ .
- **R-C3D** [37] runs at the same speed: 569fps on an NVIDIA Titan X Maxwell GPU and 1030fps on an NVIDIA Titan X Pascal GPU. So the average computation time to predict each video is:  
 $3254 \div 569 \approx 6\text{s}$  on Titan X Maxwell, and  $3254 \div 1030 \approx 3\text{s}$  on Titan X Pascal.
- **OBUI6** [27] uses C3D for feature extraction running at 313.9fps on the GPU, a binary random forest, and a dynamic programming process for generating proposals. So only considering the feature extraction, the average computation time to process each video is:  
 $3254 \div 313.9 \approx 10\text{s}$ .
- **UPC16** [18] consists of C3D running at 313.9fps on the GPU, and a single layer LSTM predicting with 2.7ms on the GPU. C3D uses a short video clip of 16 frames as input. So the average computation time to predict each video is:  
 $(3254 \div 313.9)\text{s} + (3254 \div 16 \times 2.7)\text{ms} \approx 11\text{s}$
- **UTS16** [32] extracts a variety of features such as iDT features, C3D features, deep features by ResNet152 (pre-trained on ImageNet), deep features by ResNet152 (pre-trained on Places2), and deep features by InceptionV3. Additional costs involve VLAD encoding of multiple features and SVM classification. So only considering the feature extraction by iDT which runs at 3.5fps on the CPU, the average computation time to process each video is:  
 $3254 \div 3.5 \approx 930\text{s}$ .
- **CDC** [23] relies on the detection outputs of UTS16 [32], i.e., it is used to refine the predicted results of UTS16. While CDC runs at 500fps in the refining process, the computation bottleneck comes from generating the temporal segments by UTS16. So the overall computation time is determined by UTS16: 930s.

## B. Illustration of Policy Execution

Figure 3 illustrates the frame selection and prediction process of the policy. Each colored box above the frame sequence shows the predicted action class (with associated probability score), and detected temporal segment (from start to end). We can directly discard the segments that are

predicted as background. At steps 2 and 3, the policy makes the true positive predictions that match to the two ground truth segments. Frames of the observing sequence present the selected frames for the corresponding steps.

## C. Examples of Detected Activities

Figure 4 demonstrates the prediction examples of our model, including the challenging classes that involve large scale change, great viewpoint variations, and crowded background.

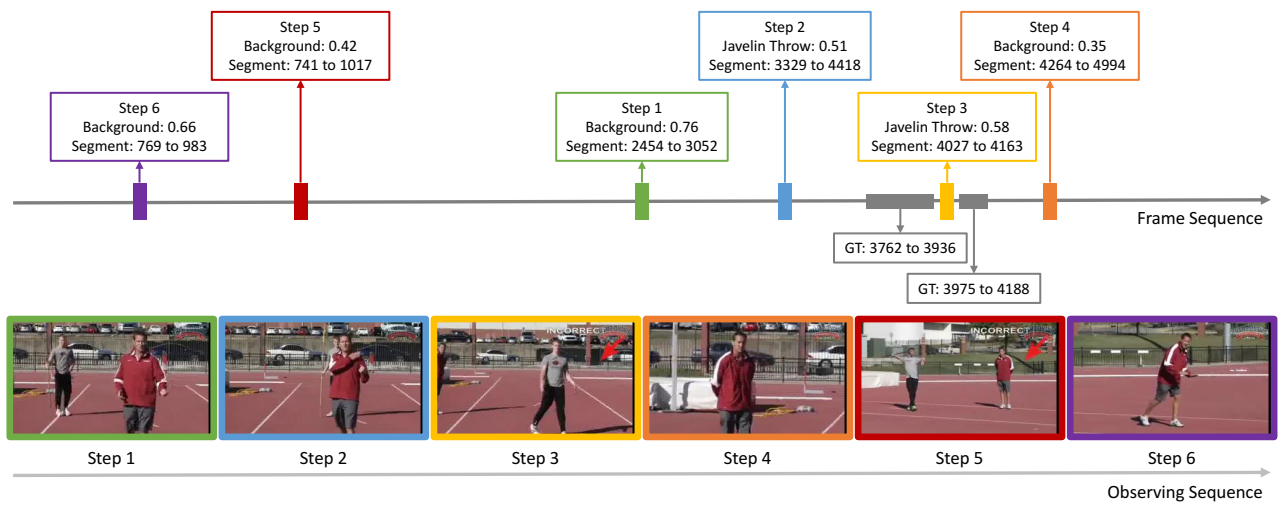


Figure 3. Example of our policy running for frame selection and action prediction on the THUMOS14 dataset.

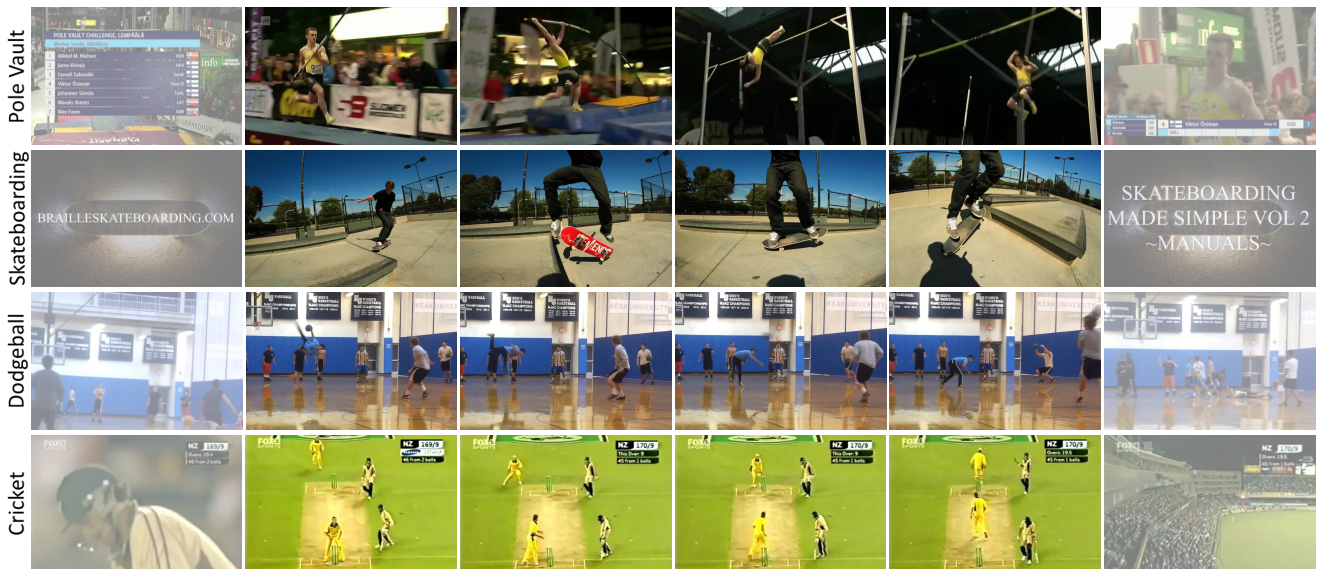


Figure 4. Examples of predicted results on the ActivityNet dataset. Each row shows four sampled frames within the temporal extent of a detected activity. Faded frames indicate the frames outside the detected temporal boundary.